

The Reproducibility of Surface Air Temperature over South Korea Using Dynamical Downscaling and Statistical Correction

Joong-Bae AHN, Joonlee LEE

Department of Atmospheric Sciences, Pusan National University, Korea

and

Eun-Soon IM

National Institute of Meteorological Research, Korea Meteorological Administration, Korea

(Manuscript received 7 July 2011, in final form 3 May 2012)

Abstract

On the Korean peninsula, observation is being conducted so densely that the mean distance between stations of the extensive ground-based data network is only 12.7 km. Nevertheless, because of significant mountainous terrain and the fact that most observation sites are situated in low areas rather than mountain tops or ridges, the detailed topographical effect on temperature distribution is not reflected properly. A model using fine-scale grid spacing can represent such a topographical effect well, but due to systematic biases in the model, simulated temperature distribution will be different from the actual observation. This study therefore attempts to produce a detailed mean temperature distribution for South Korea through a method combining dynamical downscaling and statistical correction. For the dynamical downscaling, the Weather Research and Forecast (WRF) model developed by the U.S. National Center for Atmospheric Research (NCAR) is used. We applied a multi-nesting technique to obtain high-resolution climate information (3 km) with a focus on the Korean peninsula. The integration period was 10 years from January 1999 to December 2008. For the correction of systematic biases shown in downscaled temperature, a perturbation method divided into the mean and the perturbation part was used with a different correction method being applied to each part. The mean was corrected by a weighting function while the perturbation was corrected by the self-organizing maps method, which is one of the artificial neural networks method. The results with correction agree well with the observed pattern compared to those without correction, improving the spatial and temporal correlations as well as the root mean square error. In addition, they represented detailed spatial features of temperature including topographic signals, which cannot be expressed properly by gridded observation. Through comparison with in-situ observation with gridded values after objective analysis, it was found that the detailed structure correctly reflected topographically diverse signals that could not be derived from limited observation data.

1. Introduction

Since the general circulation model (GCM) was developed several decades ago, it has been an import-

ant tool for producing weather and climate information (Meehl 1995). However, despite the successful development of GCM over the last several decades, coarse-resolution is still not adequate for providing detailed local or regional weather and climate information, particularly in such a narrow region as the Korean peninsula. Thus, recent dynamical downscaling based on the regional climate model (RCM) (Giorgi et al. 1990; Im et al. 2011) or statistical downscaling (von Storch et al. 1993; Wilby et al. 1998) has been utilized to obtain high resolution

Corresponding author: Joonlee Lee, Climate Prediction Laboratory, Department of Atmospheric sciences, Pusan National University, Gumjung-gu, Jangjeon-dong, Busan, 609-735

E-mail: leejl@pusan.ac.kr

©2012, Meteorological Society of Japan

climate information.

Although GCM and RCM are being refined continuously, it is impossible for these models to simulate and forecast nature perfectly due to errors and uncertainties in initial conditions, the model physics and parameterizations, and the complex nature of earth systems (Lorenz 1963). In order to overcome these problems, systematic biases in model results are often statistically corrected using a model output statistic (MOS) method. (e.g., Wilks 1995). Such statistic methods include linear methods such as single linear regression (SLR) (Wigley et al. 1990) and multiple linear regression (MLR) (Ahn et al. 2002) and non-linear methods such as genetic algorithm (GA) (Holland 1975; Nasser et al. 2008) and the artificial neural network method (ANN) (Schoof and Pryor 2001; Ahn et al. 2005). Due to both linear and non-linear characteristics in the mass and momentum fields of earth fluid such as the atmosphere, it is important to apply adequate methods selectively according to the nature of the variables.

The application of dynamic downscaling methods and statistic correction methods (MOS) for generating accurate and precise meteorological data has been carried out in several previous studies. Ahn et al. (2002) removed systematic biases using MLR from meteorological data (5 km) downscaled by the Mesoscale Model Version 5 (MM5) (Grell et al. 1994). However, the general conclusion from this analysis was hindered by the relatively short integration period and the particular months involved (January to April). Ahn et al. (2005) also corrected winter temperature data produced by MM5 using MLR and the multi-layer perceptron (MLP) (Rumelhart et al. 1986) method, which is an ANN method. The authors suggested that a non-linear statistic method shows better performance than a linear statistic method. In case of MLP used in the study, however, training was done using the back-propagation algorithm until the cost function became close to 0. This method has a shortcoming, however, the variance of output decreases in the process.

In this study, the detailed distribution of monthly temperatures (3 km in horizontal resolution) in South Korea was reconstructed using a dynamical downscaling and an adequate statistic correction method for the removal of systematic biases in the downscaled results. For the statistical correction, a non-linear self-organizing maps (SOM) (Kohonen 1990; Richardson et al. 2003; Robert et al. 2003) is applied to resolve the shortcomings of MLP while preserving the merits of the perturbation method and non-linear methods. Once such a methodology successfully reproduces gridded climate information with a suitably fine-scale that reflects the local climate char-

acteristics over Korea, it can help overcome the spatial and temporal limitation of ground-based observational data. Although the Korean territory is covered by a relatively dense observational network, most of the stations are situated below 300m due to restrictions in maintaining observational stations at high altitude. Therefore, a gridded observation (gridded OBS) dataset produced by simple objective analysis could yield misleading meteorological information at individual stations and filter out substantial local-scale variation possibly related to in-situ observation (in-situ OBS).

In this paper, section two explains the data and the correction method used in this study. Section three provides comparison of observations and downscaled results without and with statistical correction. Finally, a summary is provided and future research directions are discussed in section four.

2. Data and method

2.1 Dynamical downscaling

In order to reconstruct fine-scale temperature in South Korea, we performed dynamical downscaling using the Weather Research and Forecast (WRF) (Skamarock et al. 2008) Model developed by the National Center for Atmospheric Research (NCAR) with the initial and boundary conditions from National Centers for Environmental Prediction/National Center for Atmospheric Research (NCEP/NCAR) reanalysis-2 data with 6 hour intervals for the period from 1999 to 2008. Integration was restarted in every month of each year and a three-days period prior to the first day of a month was assigned as the spin-up period for each simulation. A 3-day spin-up period is sufficient for dynamical adjustment between lateral forcing and the internal physical dynamics of a model (Hong et al. 2009; Wilson et al. 2011). We applied a multiple nesting technique, including three domains with horizontal grid spacing of 27 km, 9 km and 3 km centering on South Korea. The analysis is only focused on the monthly temperature derived from the third domain; that is the 3km resolution over the southern part of the Korean peninsula (125°E–130°E, 34°N–38.5°N). The model configurations are shown in Table 1 and a more detailed explanation is described by Ahn et al. (2009).

2.2 Statistical correction

Model output (A_m) may be decomposed as follows:

$$A_m = (A + \epsilon_{random}) + \epsilon_{model}$$

where A is a signal (or a true value), ϵ_{random} is model error due to incompleteness of the model and ϵ_{model} denotes the errors associated with the chaotic nature of

Table 1. Summary of the configuration for the WRF multi-nesting system used in this study

ARW solver		Description
Center point		Seoul metropolitan
Horizontal (Vertical) resolution of Domain 1		27km × 27km (28level, Grid # - 189 × 152) 104.37°E~150.03°E, 21.051°N~50.196°N
Horizontal (Vertical) resolution of Domain 2		9km × 9km (28level, Grid # - 213 × 201) 118.62°E~135.78°E, 30.162°N~43.097°N
Horizontal (Vertical) resolution of Domain 3		3 km × 3 km (28level, Grid # - 222 × 222) 124.34°E~130.30°E, 33.845°N~38.652°N
Physical scheme	Microphysics	WRF Single-Moment 6-class scheme (Hong and Lim 2006)
	Cumulus	Kain-Fritsch scheme (Kain and Fritsch 1990, 1993)
	Planetary boundary	Yonsei University scheme (Hong and Dudhia 2003)
	Land surface model	Noah land surface model (Ek et al. 2003)
	Shortwave radiation	Dudhia scheme (Dudhia 1989)
	Longwave radiation	Rapid Radiative Transfer Model (Mlawer et al. 1997)

the atmosphere including errors in observation, etc.

Typically, the ϵ model can be subdivided into two parts: systematic and non-systematic biases. Since systematic biases show a regular pattern, they tend to be effectively reduced, indicating a large correction effect even when using a simple statistical method. On the other hand, non-systematic errors occur with neither well-defined patterns nor natural preferences; therefore, it is very difficult to extract non-systematic error from the simulation. Considering these basic characteristic differences between systematic and non-systematic biases, we attempt to correct for systematic bias using appropriate statistical methods.

Systematic biases are defined as the mean state difference between the model and observation. We divided systematic bias into two components: mean and perturbation. These two biases are statistically corrected separately in this study. Previous studies have estimated the mean and perturbation systematic biases using different procedures (Feddersen et al. 1999; Ahn et al. 2002). This is because, even though the effect of perturbation is less dominant compared to that of the mean, we can obtain more reasonable results in terms of variation through the application of a non-linear statistical approach for the perturbation bias due to its non-linear behavior.

This study assumed that simulated data can be closer to the “true” value through the removal of such systematic biases by statistical correction. For the correction, we first divided the model data (A_m) and the observed data (A_0) into the mean part (\bar{A}_m , \bar{A}_0) and the perturbation part (A'_m , A'_0) using the perturbation method:

$$A_m = \bar{A}_m + A'_m$$

$$A_0 = \bar{A}_0 + A'_0$$

The difference in the mean parts of the model and observation was defined as \bar{A}_d , and \bar{A}_{m1} was obtained by subtracting \bar{A}_d from the mean part of the model. In addition, the mean values averaged over a land area in a third domain from the mean parts of the simulation and observation were defined a_m and a_0 , respectively, and \bar{A}_{m2} was obtained by the sum of the mean part of the model and the mean value difference averaged over the target area of the model to observation. \bar{A}_{m1} , which is equal to the mean part of observation, was used for spatial distribution close to the actual value, and \bar{A}_{m2} was used in order to provide detailed topography.

$$\bar{A}_d = \bar{A}_0 - \bar{A}_m$$

$$\bar{A}_{m1} = \bar{A}_0 = \bar{A}_m + \bar{A}_d$$

$$\bar{A}_{m2} = \bar{A}_m + (a_0 - a_m)$$

Finally the corrected mean \bar{A}_{nm} is obtained by giving weights to the mean \bar{A}_{m1} and \bar{A}_{m2} , and model value \bar{A}_m .

$$\bar{A}_{nm} = W_1 \times (\bar{A}_{m1} + \bar{A}_{m2}) / 2 + W_2 \times \bar{A}_m$$

$$W_1 = 1 - W_2, W_2 = e^{-\{(H-350)^2 + (H-350)^2/8\}}$$

These weights are used for correction since temperature distribution along an altitude cannot be represented properly in the gridding of observed data. Here, the weights, W_1 and W_2 are expressed as the function of height, and the Gaussian function is used for W_2 . H is the height of input data.

For correction of the perturbation (A'_m), the SOM, one of ANNs, is used. The structure of the SOM meth-

od has two layers, namely, the input and output layers. Input data (P_i) indicates the pattern to be trained, whereas the output layer is a pattern map created through the training of input data. Each neuron in the output layer has an arbitrary weight (W_i) for all input data.

The SOM algorithm starts by assigning an arbitrary number to an arbitrary weight of each neuron in the output layer. According to Kohonen's learning rule (Kohonen 1990), similarity between the created arbitrary weight and input data is calculated using Euclidian distance.

$$Distance = \sqrt{\sum_{i=1}^n (P_i - W_i)^2}$$

In this method, the smallest value, namely the value that has the shortest distance is called the "winner neuron."

$$W_i(\text{new}) = W_i(\text{old}) + B(P_i - W_i(\text{old}))$$

This neuron is given an opportunity to train for input data, and adjusts the weight strength of the neuron. Here, B means the learning rate. The learning rate controls the rate when we update the winner neuron's weight calculated by Euclidian distance in Kohonen's learning rule. When the learning rate is large, there is an advantage of a faster training speed but a disadvantage of lower accuracy, and vice versa in the case of a small learning rate. Barring the winner neuron, similar neurons within the neighborhood radius of the winner neuron are adjusted using a Gaussian function. As the distance from the winner neuron is closer, the similar neurons are learned with higher weighting. The neighborhood radius and the learning rate are reduced gradually as the training proceeds. This study uses a non-linear Gaussian function, which has been used in many previous studies, as the weighting to remove the perturbation part of the bias to give similarity with non-linear natural variation.

This study used the perturbation value (A'_m) of a model with 222×222 grids and the perturbation value (A'_0) of observation as input data. We assume, however, that the perturbation bias does not strongly depend on the topographical effect. In fact, the temporal correlation coefficients for each month between in-situ OBS and gridded OBS re-interpolated to the in-situ observational site are still quite high (close to 1) (results not shown). Thus, we assumed that gridded observation is used for the training input data of the SOM. Therefore, although the gridded OBS includes errors induced by horizontal interpolation, we assume that the gridded OBS could substitute the perturbed part of true values. The arbitrary weight of each neuron in the output layer was given the

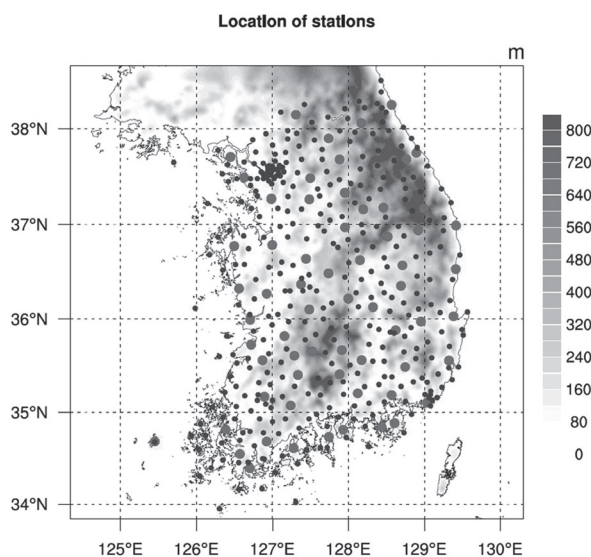


Fig. 1. Topography (m) and distribution of 70 ASOS (large dots) and 345 AWS (small dots) used in analysis of observation data.

same dimension as input data. That is, the equation to obtain Euclidian distance is expressed as follows:

$$Distance = \sqrt{\sum_{j=1}^{222} \sum_{i=1}^{222} (P_{nj} - W_{sj})^2}$$

Here, i and j indicate the number of spatial grids. After winner neurons were obtained, a neighborhood radius was selected rectangularly, and the winner neurons were trained according to Kohonen's learning rule. Here the initial learning rate was assigned as 0.3 and a Gaussian function was used as a radius adjustment function. From the pattern map completed through the training, we found the values closest to observation using Euclidian distance and used these values for correction.

2.3 Observation dataset

Automated surface observation systems (ASOS) and automatic weather stations (AWS) data from 1999 to 2008 provided by Korea meteorological administration (KMA) is used for the observation. Figure 1 shows observation sites on a map of the southern part Korean peninsula. Large and small dots indicate the locations of 70 ASOS and 345 AWS stations, respectively. As shown in the topography (GTOPO30 data by USGS/EROS, horizontal grid spacing of 30 arc seconds, approximately 1 kilometer), the Korean peninsula is characterized by a physiographical feature in which mountain peaks and valleys are sharply defined. Therefore, even though

Table 2. General information about the distance and height from the observation sites and the model grid system.

	Mean distance	Max distance	Min distance	Mean Height	Max Height
ASOS	32.6 km	142.3 km	13.7 km	109.8 m	842.5 m
AWS	13.9 km	132.1 km	2.0 km	117.0 m	968.3 m
ASOS+AWS	12.7 km	53.6 km	0.4 km	115.8 m	968.3 m
Model	3.0 km	3.0 km	3.0 km	215.3 m	1262.8 m

there is a dense observation network of more than 400 distributed sites, these are not sufficient to represent the significant fine-scale details. The average distance between ASOS sites is 32.6 km and 142.3 km at maximum (see Table 2). However, these values are reduced to 12.7 km and 53.6 km once the AWS sites are added to the ASOS sites.

For comparison with the simulation using gridded values, observations at station-base are converted into the same gridded system of the simulation (3 km) using Cressman objective analysis (Cressman 1959). In the converting procedure, the effective radiuses are assigned as 15 km and 30 km for ASOS and 6 km and 12 km for ASOS + AWS. Despite the dense observation network, the process to convert station data into gridded data includes the possibility of an inaccurate reflection of the topography effect because the mean distance between the observation sites is still too large compared to model grid spacing. More detailed explanation of this follows in section three.

3. Results

3.1 Analysis of temperature field in the Korean Peninsula

Figures 2 and 3 show spatial distributions for the 10-year (1999–2008) average temperature derived from the gridded ASOS, the gridded ASOS+AWS, the simulation without correction (U_WRF), and the simulation with correction (C_WRF) for May and November. By comparison with ASOS + AWS, temperature distribution of ASOS generally follows the broad pattern of ASOS + AWS, however the topographical effect became much smoother because the mean distance between ASOS sites is almost three times greater compared to that of ASOS + AWS. The mean distance is lessened by adding AWS sites, which makes temperature distribution relatively more precise. However, this interval is still not sufficient in expressing the detailed characteristics of the temperature field over South Korea, which has complex topography. Moreover, most of the observation sites are not located along ridges in the mountainous area as shown in Fig. 1, and their altitude is low; therefore, observational data collected from such

sites may not represent the average distribution of temperature in South Korea. That is, because temperature decreases adiabatically with altitude, the mean temperature distribution obtained from ASOS or ASOS+AWS observation does not adequately show the topographical effect. Additionally, the values are usually higher than the actual mean temperature because most of the observation sites are low in altitude. Although meteorological observation in South Korea is performed more densely than that in many other countries, it is still insufficient to express temperature distribution over the region's complex topography, around 70% of which comprises mountainous terrain.

On the contrary, the results simulated by the high-resolution numerical model (WRF) with a horizontal grid resolution of 3km express the better temperature distribution for mountainous terrains such as the northeastern region (Figs. 2c, 3c). However, the model results reveal the systematic biases across the entire region, indicating the underestimation (overestimation) for the warm (cold) season. One of key ideas derived from this figure is that the simulated distribution reflects the effect of elevation. The low and high temperatures along the high and low elevations, respectively, are relevant. This, in turn, provides the possibility of realistic high-resolution simulation for regional or local temperature fields if the systematic biases are to be reduced or removed.

Figures 2d and 3d show the temperature distribution of the C_WRF. The correction method preserves the advantage of dynamical downscaling, which can express details and simultaneously corrects systematic biases in the model so that the model can produce more accurate simulation results. That is, as systematic biases are removed from the model, the overall pattern and mean value of observation (ASOS + AWS) are better simulated and temperature distribution reflecting topographical effects is expressed in detail. In the case of May, the mean temperature is 15.0°C in the regional climate model (U_WRF), but becomes 16.8°C after correction (C_WRF). That is, the negative bias has been corrected and, as a result, the simulation result is closer to observational data (17.0°C in ASOS, 16.8°C in ASOS + AWS). On the contrary, the downscaled temperature is relative-

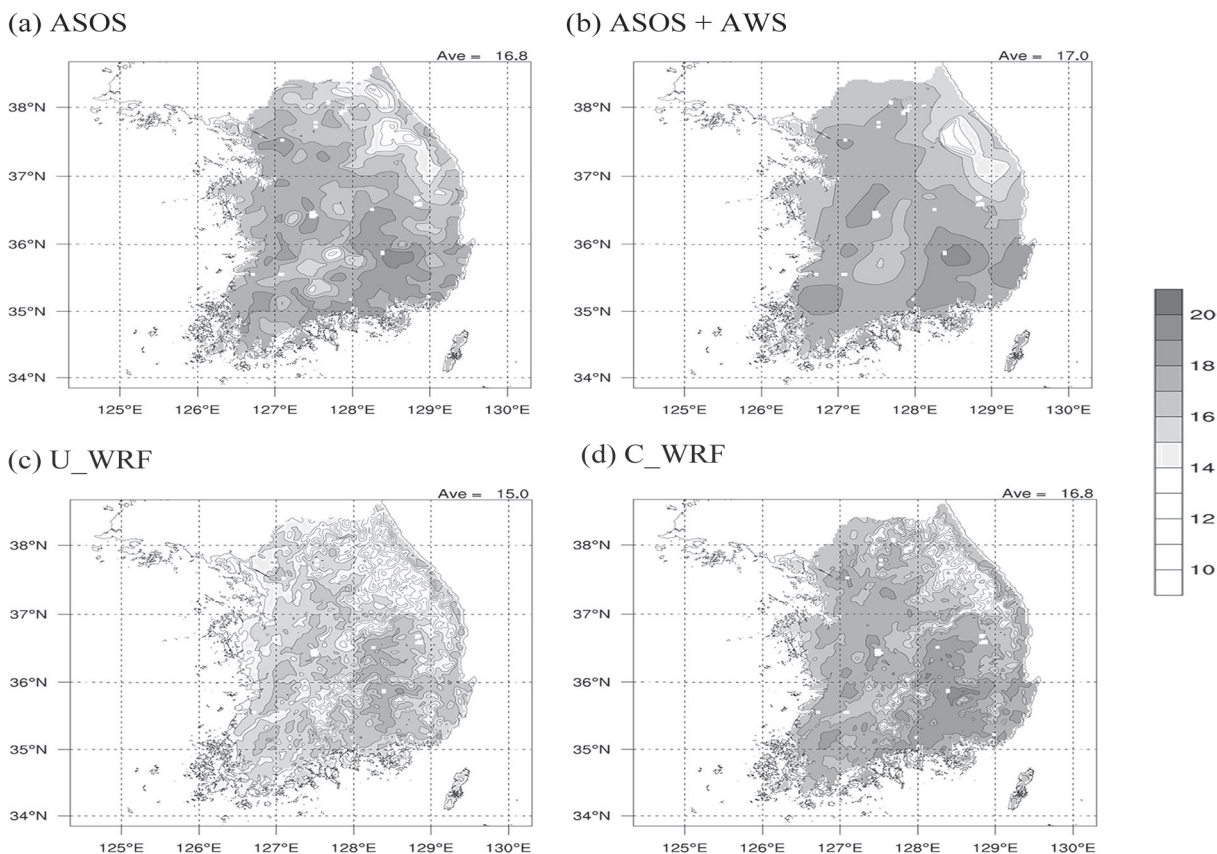


Fig. 2. Distribution of surface air temperature over South Korea for May, averaged over ten years (1999–2008) derived from the ASOS data (a), ASOS + AWS (b), U_WRF (c), and C_WRF (d).

ly higher than that of the observation for the southern region in November. The mean temperature of the Korean Peninsula is 7.7°C before correction (U_WRF) but 6.6°C after correction (C_WRF), indicating that the bias of a high simulated temperature was corrected, making the simulated temperature closer to the observational data (7.1°C in ASOS, 6.7°C in ASOS + AWS).

Figure 4 comprehensively shows the monthly mean temperature averaged over South Korea. The annual mean temperatures of South Korea are 12.2°C and 12.0°C , respectively, when using ASOS and ASOS + AWS. Considering that the mean altitudes of ASOS and AWS observation sites are 109.8 m and 117.0 m, respectively, it is believed that as the number of observation sites increases, the mean altitude of observation sites also increases and, as a result, observed temperature were around 0.2°C lower. Moreover, the mean temperature simulated by WRF was 0.8°C lower than that in ASOS + AWS, mainly because of systematic biases in the mode; more specifically because temperature was

simulated at lower values for most months except some in the cold season. In C_WRF, the mean temperature of South Korea is given as 11.9°C , which is higher than the 11.2°C of U_WRF and lower than the 12.0°C for ASOS + AWS. This suggests that the cold bias in U_WRF was appropriately corrected. At the same time, considering that the mean altitudes of ASOS + AWS and WRF grids are 115.8 m and 215.3 m respectively, we can see that the decrease in temperature resulting from the topographical effect was expressed adequately. That is, the result after correction is smaller than observational data values (ASOS + AWS) because the C_WRF expresses the landform in detail and, accordingly, reflects the change of temperature with altitude well. In other words, it reflects the fall of temperature as altitude increases above sea level that results from the topographical effect.

3.2 Analysis of temperature field in a mountain area

In order to examine temperature difference caused by the topographical effect, this section focuses on the

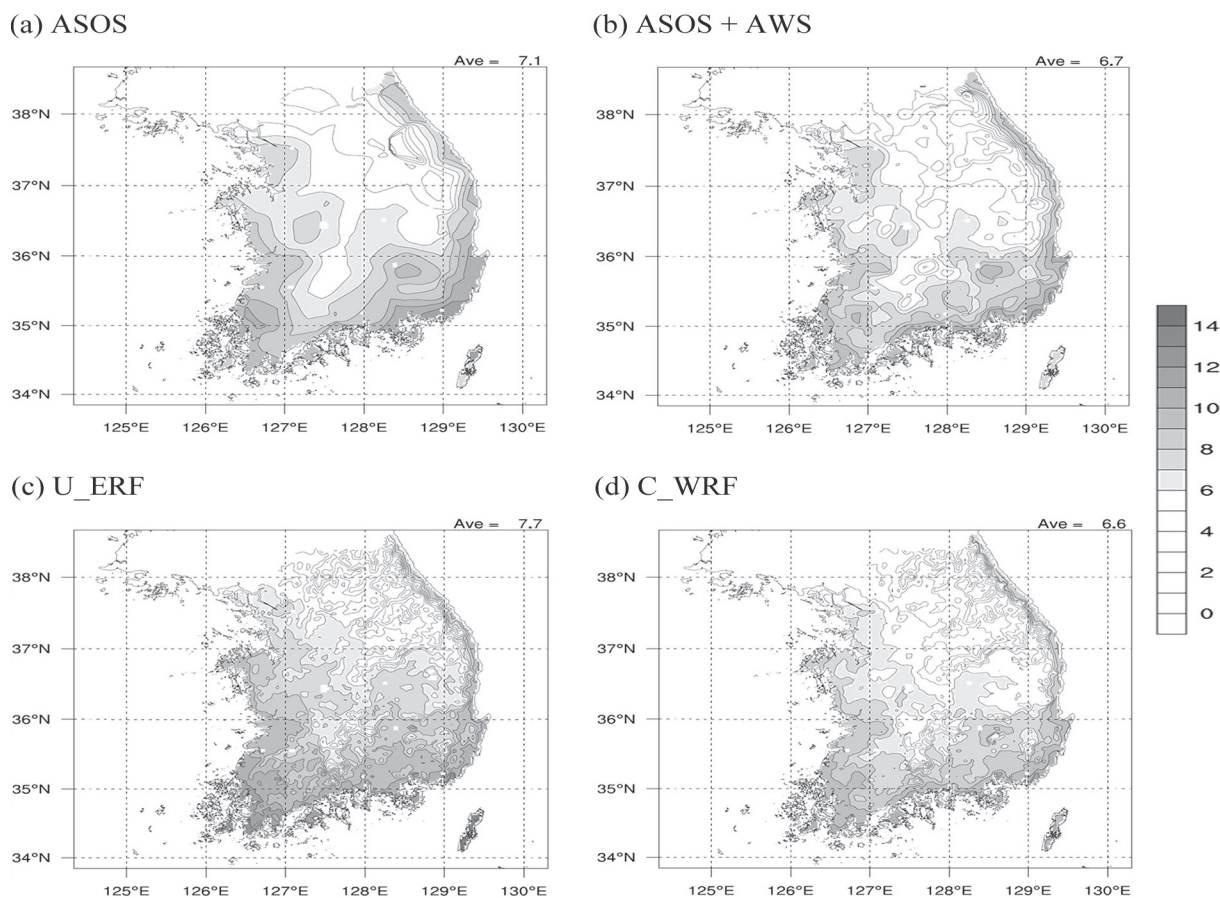


Fig. 3. As in Fig. 2, but for November.

temperature of the mountainous northeastern region of South Korea. Figure 5 shows the temperature distribution of a mountain area in Gangwon-do for April. As in Fig. 1 few of the ASOSs (large dots) are on the ridge of a mountain, whereas some of the AWSs (small dots) are in mountains but are also not on ridges. Accordingly, when the mean temperature field is drawn using data from ASOS or ASOS + AWS, temperature distribution along the ridges of mountains largely disappears as shown in Figs. 5a and 5b. Particularly because there is no observation site along the Sobaek Mountains between 128°50'E, 37°05'N to 127°50'E, 36°30'N, temperature in this area is interpolated by data observed at surrounding lower sites and, as a result, it appears to be flat. That is, temperature distribution obtained from ASOS + AWS does not reflect the landform of mountains. In comparison, the U_WRF reflects the topographical effect well, but due to its systematic biases, the model simulates temperature lower than those from observational data.

As explained in the previous section, however, the C_WRF effectively expresses the overall pattern found in observation as well as detailed temperature distribution throughout the landform.

Using the temperature field in Fig. 5, we presented the distribution of temperature according to the altitude (Fig. 6). The figure shows temperature from in-situ OBS without gridding (ASOS + AWS), gridded OBS (ASOS + AWS), the U_WRF, and the C_WRF. In-situ OBS used 87 temperature values, whereas gridded OBS expressed 5925 temperature values in the function of altitude. In general, temperature decreases with increasing altitude and this characteristic is reflected well in the graph. In Fig. 6, the lapse rate shown in in-situ well represents temperature's strong dependence on elevation. Temperature decreases as elevation increases without large deviation. However, gridded OBS reveals the deficiency of horizontal interpolation. Due to a smoothed or inflated topographical effect, the distribution was not

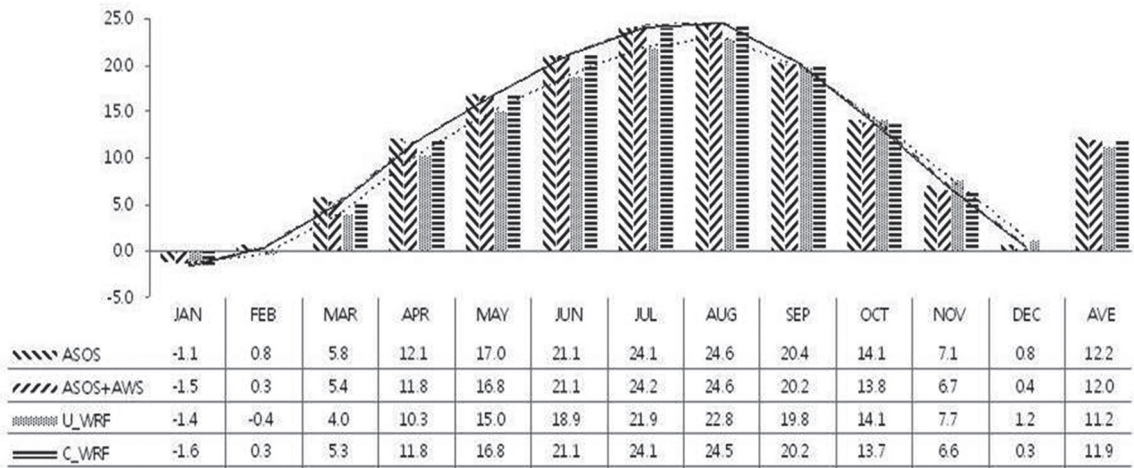


Fig. 4. Summary of the monthly mean temperature averaged over South Korea derived from the ASOS (right diagonal line), ASOS + AWS (left diagonal line), U_WRF (dotted line) and C_WRF (line).

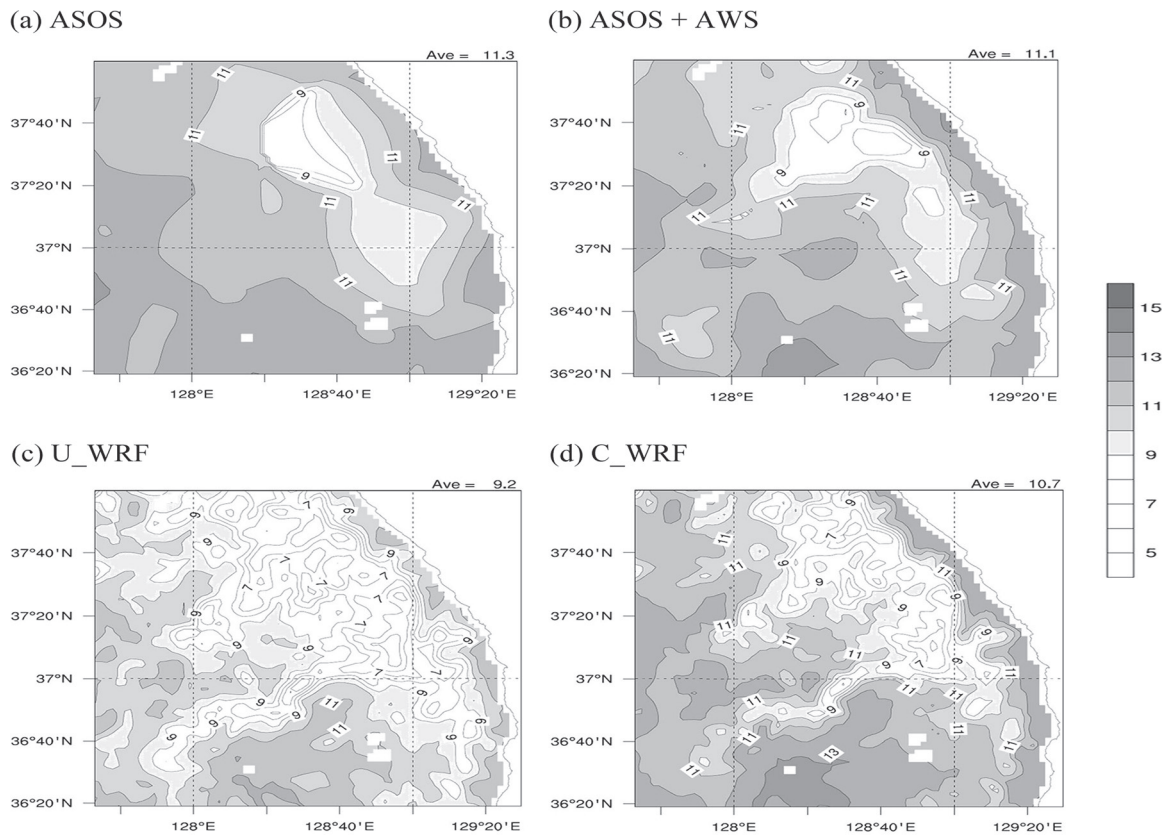


Fig. 5. Distribution of surface air temperature over the Kangwondo mountainous area for April, averaged over ten years(1999~2008) derived from the ASOS data (a), ASOS + AWS (b), U_WRF (c), and C_WRF (d) .

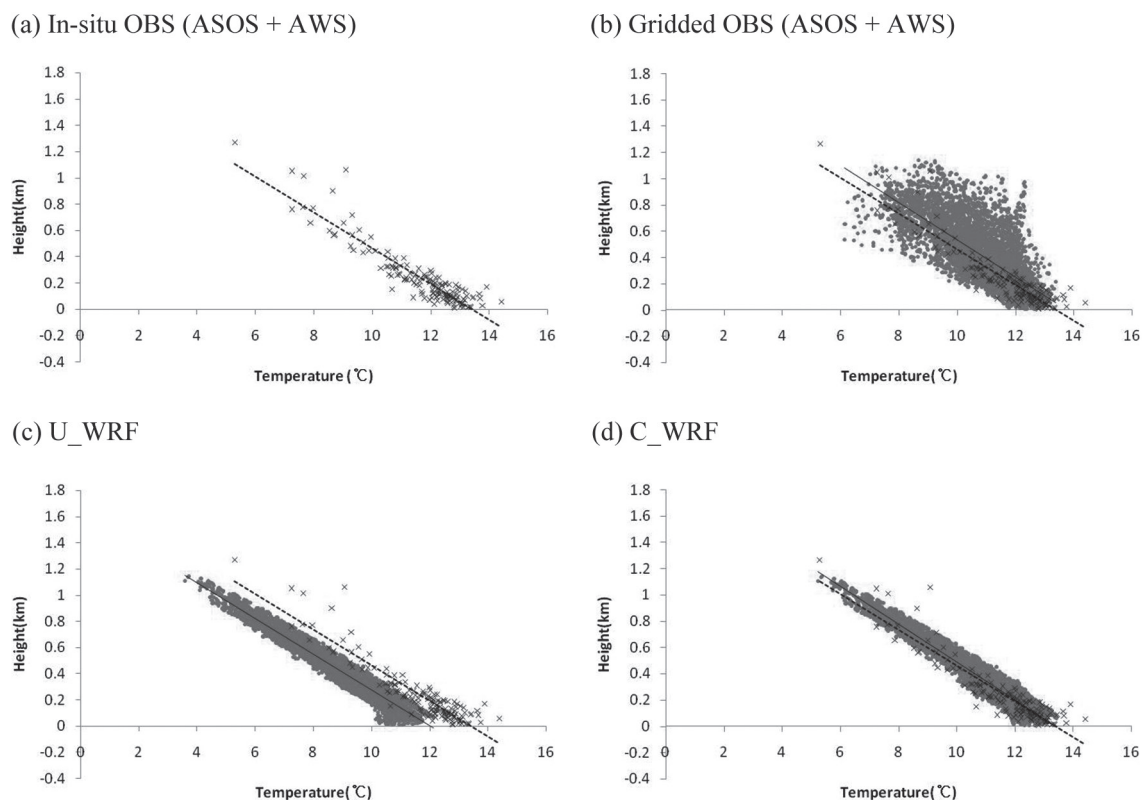


Fig. 6. Scatter plots of altitudes against surface air temperature over the Kangwondo mountainous area for April, averaged over ten years(1999~2008) derived from in-situ ASOS + AWS (a), gridded ASOS + AWS (b), U_WRF (c), and C_WRF (d). Here, all panels include the distribution of in-situ ASOS + AWS (cross) and its regression line (dotted line) for reference.

well organized as the function of elevation, showing a more widely scattered pattern. That is, temperature fluctuates more widely in the same altitude because the effect of altitude in a complex landform is not considered in the interpolation and extrapolation processes. In terms of model results (U_WRF), temperature distribution tends to follow the general behavior of in-situ OBS, showing roughly linear decreases in temperature with elevation, even though the model tends to underestimate temperature, compared to observation data. After applying the correction method, the systematic underestimation biases mostly disappear. The regression line of C_WRF shows good agreement with in-situ OBS, with a coefficient of determination R^2 closer to 1. Therefore, C_WRF reasonably reflects altitudinal distribution in spite of smoother gridded topography than the reality. The detailed procedures of the statistical correction involved are described in Subsection 2.2.

Figure 7 shows the temperature differences among 415 in-situ OBS, gridded OBS, and regional climate

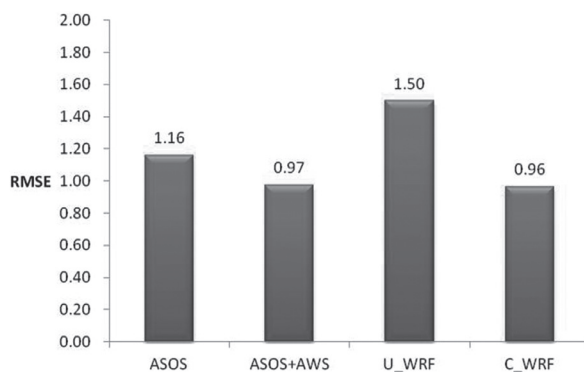


Fig. 7. Root mean square error of annual mean surface air temperature between In-situ OBS (AWS + ASOS) and OBS (ASOS + AWS), U_WRF, and C_WRF.

models before and after correction (U_WRF, C_WRF). In the 12-month averages of in-situ OBS, the difference was 1.16°C with ASOS, 0.97°C with ASOS + AWS,

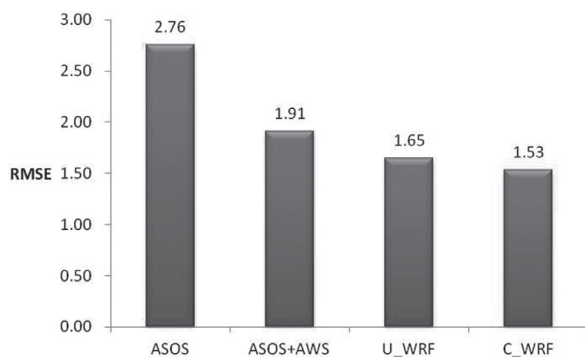


Fig. 8. As for Fig. 7, but for heights above 350 m.

1.50°C with U_WRF, and 0.96°C with C_WRF. The regional climate model (U_WRF) showed the largest difference from in-situ observation, but after correction this difference was reduced and became even smaller than that in ASOS+AWS.

In order to further examine the topographical effect, we analyzed temperature difference at in-situ OBS sites over 350 m in altitude (Fig. 8). In the U_WRF, which showed the largest difference in Fig. 7, the difference was 1.65°C, smaller than the 1.91°C in ASOS+AWS. The difference was 1.53°C the smallest in the C_WRF. The reason that the WRF result showed a smaller temperature difference than that of ASOS+AWS at observation sites over 350m in altitude is that, as shown in Fig. 6, WRF effectively expresses the change and variance of temperature according to altitude.

Summarizing results, considering corrected spatial pattern, temperature distribution as a function of altitude and comparison with in-situ OBS, the 10-year mean temperature field given by C_WRF is more precise and closer to in-situ OBS than that of the gridded OBS (ASOS+AWS).

3.3. Analysis of variation

In the previous section, we examined the spatial distribution of 10-year mean temperatures obtained from gridded OBS and simulation, before and after correction. This section validated the results using analysis methods such as the anomaly correlation coefficient (ACC), pattern correlation coefficient (PCC), root mean square difference between model simulations and gridded OBS (RMSD), standard deviations (STD), normalized standard deviations (NSTD) and a Taylor diagram. Figure 9 shows PCC-RMSD, which comprises 10-year means for each month. The square indicates the U_WRF, whereas the circle indicates the C_WRF. A high PCC indicates

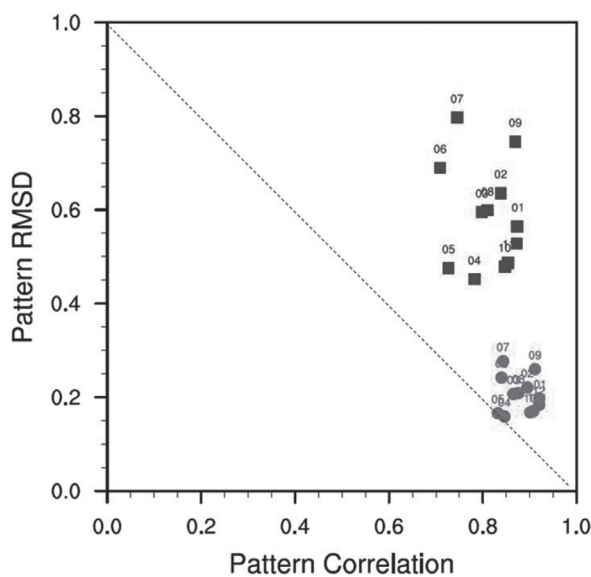


Fig. 9. Pattern correlation coefficient versus root mean square difference from gridded OBS (PCC - RMSD) of annual mean temperature derived from U_WRF and C_WRF over Korea. Here, square and circle indicate U_WRF and C_WRF, respectively.

better expression of spatial patterns, and a low RMSD indicates higher similarity with gridded OBS. The circle moved to area below the square at the right. This means that, after correction, the difference from gridded OBS became smaller and the spatial distribution pattern of temperature was better simulated, although the gridded OBS is not “true value”. Further study on the physical and/or dynamical reasons for the systematic cold bias in the spring and summer and warm bias in the winter is necessary.

Figure 10 shows an anomalous surface air temperature field expressed arbitrarily for April 2007. Compared to ASOS, the ASOS+AWS shows a more detailed temperature anomaly distribution, and C_WRF after correction expresses such a complex temperature distribution better than U_WRF. Figure 11 shows the area mean of PCC in a time series of 120 months from January 1999 to December 2008. The square indicates U_WRF, and the circle indicates C_WRF. The mean for the entire period is 0.55 in U_WRF and 0.95 in C_WRF. This means that, after correction, the air temperature PCC anomaly was improved for all the months.

Figure 12 shows a Taylor diagram representing anomalous surface air temperature. The number above each dot shows the month, and the square indicates U_WRF and the circle indicates C_WRF. In addition, data with

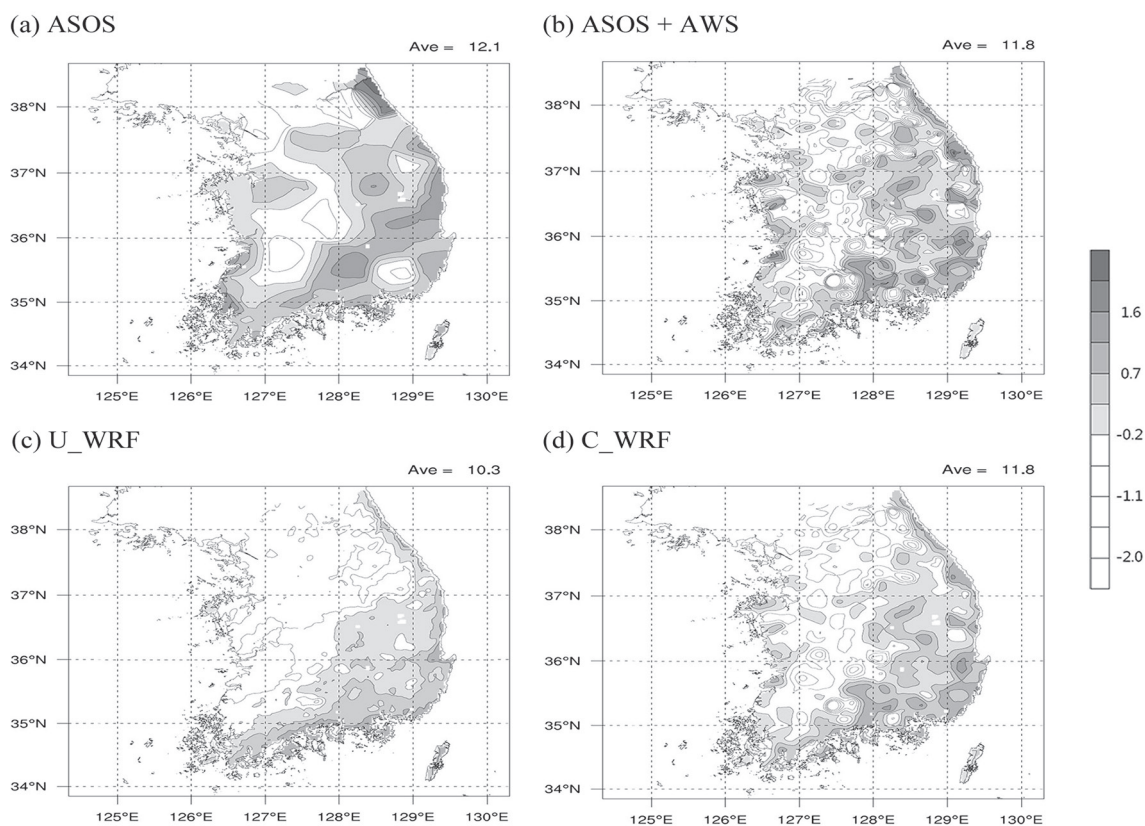


Fig. 10. As in Fig. 2, but for anomalies in April, 2007 with respect to the mean of the 10-year average.

significance levels of 95% and 99% are drawn. U_WRF shows results below the 95% significance level for May, June, July and September, whereas all the CC of C_WRF after correction are above the 99% significance level. For the NSTD, it falls within the range of 0.75–1.25 after correction. Thus, the statistical correction method used in this study is useful for expressing variation similar to observational data by improving the temporal variation of the temperature anomaly and the size of change.

Table 3 summarizes the 12 month means for the CC, STD and RMSD of anomalous surface air temperature. CC was 0.75 in U_WRF but was enhanced by 0.21 to 0.96 in C_WRF, and RMSD decreased by 0.36 from 0.57 in U_WRF to 0.21 in C_WRF. In addition, when OBS (ASOS+AWS) was 1.11, the STD was 1.08 in U_WRF and somewhat lower (1.04) in C_WRF. Accordingly, this correction can be shown to markedly improve not only the detailed mean distribution of temperature but also the variation of the model over time. It is therefore highly applicable in model-based prediction and

simulation.

4. Discussion and conclusions

In the Korean peninsula, observation is conducted so densely that the distance between observation sites, including ASOSs and AWSs, is only 12.7 km. Nevertheless, around 70% of the region is mountainous terrain and most of the observation sites are situated in low-lying areas for convenient maintenance and power supply availability rather than around mountain tops or ridges. For this reason, topographical features are poorly reflected in the gridding process of in-situ OBS. On the contrary, the result from the high-resolution regional climate model represents the pattern of temperature according to altitude well because the model takes such topographical effects into account. Due to systematic biases in the model, however, the general temperature distribution is sometimes far different from that seen in actual observation. Thus, this study removed systematic biases from the simulated results, thereby taking advantage of the high-resolution model.

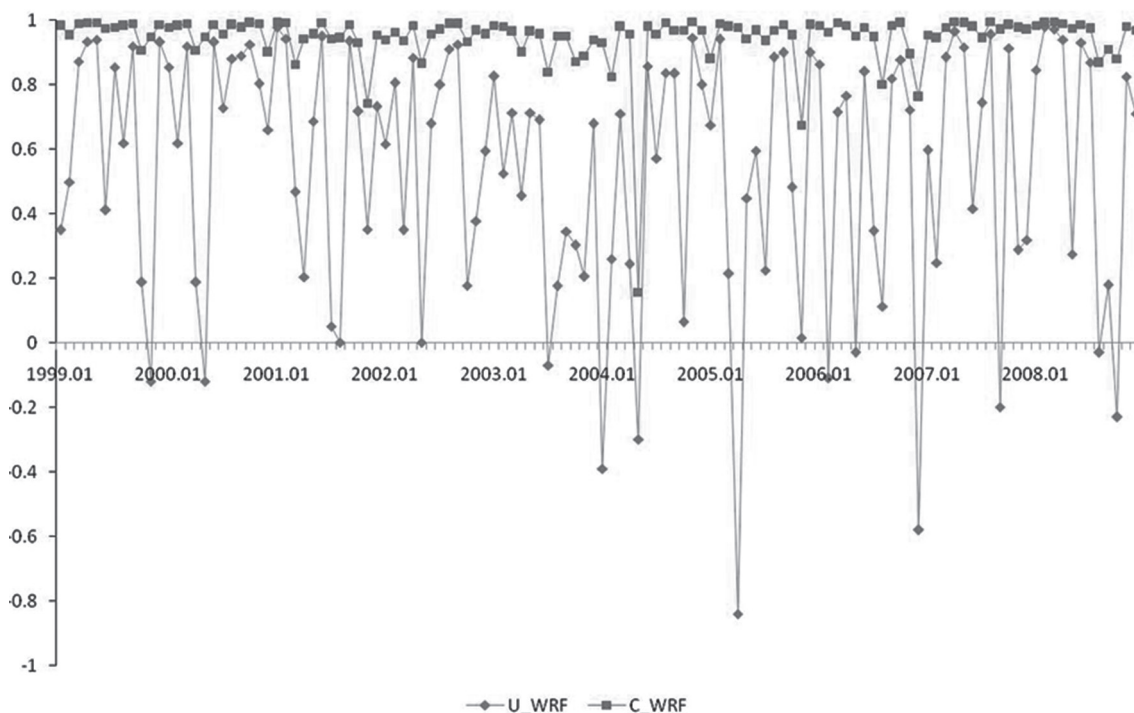


Fig. 11. Time series of pattern correlation coefficient of anomaly surface air temperatures over South Korea for January to December, 1999~2008. Here, diamond and rectangle indicate U_WRF and C_WRF, respectively.

In order to generate detailed temperature data for the Korean peninsula, this study integrated data from a 10 years period from January 1999 to December 2008, using NCEP/NCAR reanalysis data as the initial and boundary conditions of the regional climate model WRF. For observational data, we used ASOS and AWS data from 1999 to 2008 provided by the KMA.

Statistical correction in this study was largely performed by the perturbation method, dividing temperature into mean and perturbation values. Mean values were obtained by averaging the value representing the spatial distribution of observations and the value representing spatial distribution in consideration of the detailed landform of the model, and weight was given to the model according to altitude in order to reflect the change of temperature caused by landform more accurately. Perturbation values are calculated by non-linear statistical methods. The statistical method used in this study was a type of SOM, an ANN technique, which was developed for this study. From the results of testing various linear and non-linear methods (e.g., SLR, ANN(M-LP), GA) along with the SOM through cross-validation (results not presented), the SOM developed in this study produced the best results so it was used as the correc-

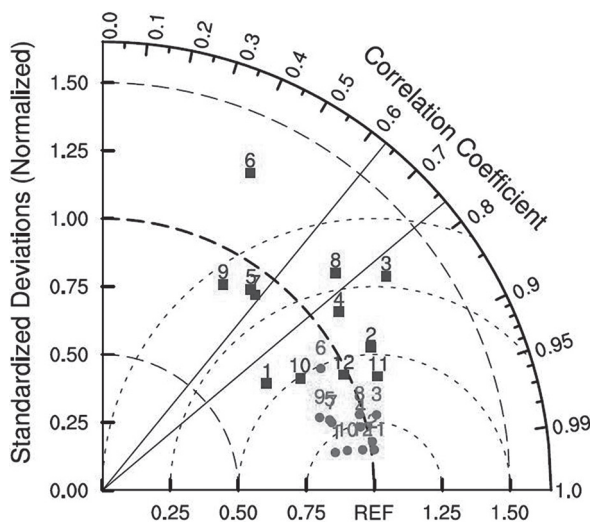


Fig. 12. Taylor diagram of anomaly surface air temperature over South Korea for January to December, 1999~2008. Here, square and circle indicate U_WRF and C_WRF, respectively. The number above the dot indicates the month.

Table 3. Annual mean basic statistics for the correlation coefficient (ACC), standard deviation (STD) and root mean square difference from gridded OBS (RMSD) derived from anomaly surface air temperature of U_WRF and C_WRF over South Korea.

	U_WRF	C_WRF
Correlation Coefficient	0.75	0.96
Standard deviation(OBS = 1.11)	1.08	1.04
Root mean square difference	0.57	0.21

tion method. In general, SOM classifies certain data according to characteristic or pattern while reducing the dimensions. Using this feature, this study created a perturbation value pattern map of observations and the model, and then chose adequate patterns and used them in correction.

The corrected mean temperature distribution showed a general pattern similar to observational data and, at the same time, reasonably expressed detailed temperature according to altitude. The mean annual temperature of South Korea was 11.2°C in the model, which was 0.8°C lower than observational data due to systematic biases in the model. After the application of systematic bias correction methods, the corrected temperature was 11.9°C, which was 0.1°C lower than the observational data value. This is because the mean altitudes of the observations and the model were 115.8 m and 215.3 m, respectively, thus the effect of the temperature lapse rate caused by the difference in altitude was reflected properly.

In order to examine in detail the effect of the temperature lapse rate according to altitude, we focused on the northeastern mountainous region. In the vertical temperature distribution according to altitude, gridded OBS showed a large variation in temperature according to altitude because it could not accurately express the landform, however the corrected temperature distribution showed small variation and was similar to the distribution (gradient) of in-situ OBS temperature. But the lapse rates from gridded simulation and the regressed in-situ observations differ slightly from each other as shown in the figure. Foehn phenomenon can be one of the reasons for the discrepancy since the area is strongly affected by foehn all year round. The lapse rates over the leeward and windward sides of mountain ranges can differ depending on the direction of winds to the ranges. Secondly, the difference may be attributed to the inhomogeneous distribution of in-situ ASOS+AWS situated mostly at relatively low altitude below mountain ridges. Thus, the lapse rate obtained from is difficult to consider

representative of the region. However, further study is necessary to understand the discrepancy.

The annual mean RMSEs of the gridded OBS, model and the bias-corrected temperature with in-situ OBS temperature were 0.97°C, 1.50°C, and 0.96°C, respectively. Thus, the corrected model showed a smaller difference than did gridded OBS. Also, the RMSEs for the observation sites over 350m in altitude were 1.91°C, 1.65°C and 1.53°C, respectively. Again, the corrected model showed the smallest RMSE while gridded OBS showed the largest RMSE. As mentioned earlier, this is because the inadequate reflection of the detailed topographical effect in the temperature of gridded OBS was represented properly by dynamic downscaling and statistical correction. Furthermore, when the variation of anomaly temperature before and after correction was examined, CC was 0.75 in U_WRF but was improved by 0.21 to 0.96 in C_WRF, and RMSD decreased by 0.36 from 0.57 in U_WRF to 0.21 in C_WRF. STD was 1.11 in OBS (ASOS+AWS), and somewhat lower as 1.08 in U_WRF and 1.04 in C_WRF. Summing up these results, when systematic biases were removed through proper statistical correction, the simulated temperature spatial variation closely followed terrain height, and seems to resolve topography issues better than the observation network data

The size of systematic bias in the model was different between months, and the larger the difference was the higher the correction effect. In the case of the corrected mean temperature field, the application of a correction method to mean values had a larger effect than the application of statistical techniques to perturbation values. The commonly used mean correction method applies a difference in mean values between observation and the model, but if the observation uses a higher resolution than the model, as was the case in the data of this study, the topographical effect cannot be represented. Thus, we added two terms created using model data, and expressed the change of temperature according to the detailed landform effect and landform by giving weight to each term. However, this method is applicable to variables with small STD and strong linearity like mean temperatures, but does not produce a high correction effect for variables with relatively large STD and non-linearity such as rainfall or hourly data. Even with the same mean temperature, variation is different between months. Therefore, the correction effect may be higher if the mean temperature correction method is applied differently according to month or season.

Variation is highly affected by SOM applied to perturbation values among correction methods. In our study, results after correction were improved compared

to those before correction, which suggests that SOM is an adequate correction method. The use of SOM in correction in this study was unique. Compared to SLR, one of the existing methods, and MLP, one of the ANNs, SOM produced improved results in terms of STD, TCC and PCC. However, cross-validation was applied to predict reproduction but the results were not significantly improved because this study used 10-year data, which is a relatively short period and the input data patterns were not sufficiently diverse.

The correction method was optimized for the reproduction of detailed temperature and SOM was used predominantly for this purpose in this study. For the proper application of this correction method to different variables such as precipitation, an appropriate algorithm through various attempts related to the input data form and pattern finding after training needs to be developed and tested through goodness-of-fit analysis.

Acknowledgments

This work was funded by the Korea Meteorological Administration Research and Development Program under Grant RACS 2010-4012, and CATER 2012-3100 and 2012-3083. The authors thank the two anonymous reviewers for their helpful and constructive comments.

References

- Ahn, J. B., C. K. Park, and E. S. Im, 2002: Reproduction of Regional Scale Surface air Temperature by Estimating Systematic Bias of Mesoscale Numerical Model. *Journal of The Korean Meteorological Society*, **38**, 69–80.
- Ahn, J. B., and Y. M. Cha, 2005: A Comparison Study of Corrections using Artificial Neural Network and Multiple Linear Regression for Dynamically Downscaled Winter Temperature over South Korea. *Journal of The Korean Meteorological Society*, **41**, 401–413.
- Ahn, J. B., J. N. Hur, and C. Kim, 2009: Reproduction of Regional Scale Climate over Korean Peninsula by Correcting Systematic Bias of Regional Climate Model. *2009 Fall Conference, Daegu, Korean Meteorological Society*, 282–283.
- Anthes, R. A., Y. H. Kuo, E. Y. Hsie, S. Low, and T. W. Bettge, 1989: Estimation of skill and uncertainty in regional numerical models. *Quart. J. Roy. Meteor. Soc.*, **115**: 763–806.
- Cressman, G. P., 1959: An operational objective analysis system, *Mon. Wea. Rev.*, **87**, 367–374.
- Fedderson, H., A. Navarra, and M. N. Ward, 1999: Reduction of model systematic error by statistical correction for dynamical seasonal predictions. *J. Climate*, **12**, 1974–1989.
- Giorgi, F., 1990: Simulation of regional climate using a limited area model nested in a general circulation model, *J. Climate*, **3**, 941–2347.
- Grell, G., J. Dodhia, and D. Stauffer, 1994: A Description of the Fifth Generation Penn State/NCAR Mesoscale Model (MM5). *NCAR Tech. Note, NCAR/TN-398+STR*, 117pp.
- Holland, J. H., 1975: *Adaption in Natural and Artificial Systems*. University of Michigan Press. 228pp.
- Hong S., V. Lakshmi, E. E. Small, F. Chen, M. Tewari, and K. W. Manning, 2009: Effects of vegetation and soil moisture on the simulated land surface processes from the coupled WRF/NOAH model. *J. Geophys. Res.*, **114**, p. D18118.
- IPCC., 2007: *Climate Change 2007 – The Physical Science Basis. Contribution of Working Group I to the Fourth Assessment Report of the Intergovernmental Panel on Climate Change* [Solomon, S., D. Qin, M. Manning, Z. Chen, M. Marquis, K.B. Averyt, M. Tignor and H.L. Miller (eds.)]. Cambridge University Press, Cambridge, United Kingdom and New York, NY, USA., 634, 647, 793–795.
- Im, E. S., and J. B. Ahn, 2011: On the Elevation Dependency of Present-day Climate and Future Change over Korea from a High Resolution Regional Climate Simulation. *J. Meteor. Soc. Japan*, **89**, 89–100.
- Kohonen, T., 1990: The self-organizing maps. *Proc. IEEE*, **78**, 1464–1480.
- Lorenz, E. N., 1963: Deterministic Nonperiodic Flow. *J. Atmos. Sci.*, **20**, 130–148.
- Nasseri, M., K. Asghari, and M. J. Abedini, 2008: Optimized scenario for rainfall forecasting using genetic algorithm coupled with artificial neural network. *Expert Systems with Applications*, **35**, 1415–1421.
- Meehl, G. A., 1995: Global Coupled general circulation models. *Bull. Amer. Meteor. Soc.*, **76**, 951–957.
- Richardson, A. J., C. Risien, and F. A. Shillington, 2003: Using self-organizing maps to identify patterns in satellite imagery. *Progress in Oceanography*, **59**, 223–239.
- Robert, G. C., and B. C. Hewitson., 2003: Clustering and upscaling of station precipitation records to regional patterns using self-organizing maps(SOMs). *Clim. Res.*, **25**, 95–107.
- Rumelhart, D. E., G.E Hinton, R.J Williams, 1986: Learning representations by back-propagating errors. *Nature*, **323**, 533–536.
- Schoof, J. T., and S. C. Pryor, 2001: Downscaling Temperature and Precipitation: A comparison of Regression-based Methods and Artificial Neural Networks. *Int. J. Climatol.*, **21**, 773–790.
- Skamarock, W. C., J. B. Klemp, J. Dudhia, D. Gill, D. Barker, M. Dudhia, X. Y. Huang, W. Wang, and J. G. Powers, 2008: A description of the Advanced Research WRF Version 3, *NCAR Tech. Note, NCAR/TN-475+STR*, 113pp.
- Von, Storch, H., E. Zorita, and U. Cubasch, 1993: Downscaling of global climate change estimates to regional scales: an applications to Iberian rainfall in wintertime, *J. Climate*, **6**, 1161–1171.

- Wilks, D. S., 1995: Statistical Methods in the Atmospheric Sciences. *Academic Press*, 467pp
- Wilson, A.B., D. H. Bromwich, and K. M. Hines, 2011: Evaluation of Polar WRF forecasts on the Arctic System Reanalysis domain. Part I. Surface and upper air analysis. *J. Geophys. Res.*, **116**, p. D11112
- Wigley, T. M. L., P. D. Jones, K. R. Briffa, and G. Smith, 1990: Obtaining sub-grid-scale information from coarse-resolution General Circulation Model Output. *J. Geophys. Res.*, **95**, 1943–1953
- Wilby, R. L., T. M. L. Wigley, D. Conway, P. D. Jones, B. C. Hewitson, J. Main, and D. S. Wilks, 1998: Statistical downscaling of general circulation model output: A comparison of methods. *Water Resour. Res.*, **34**, 2995–3008